Real-Time Observation of Interference between Atomic One-Electron and Two-Electron Excitations

Henning Geiseler, Horst Rottke, Nickolai Zhavoronkov, and Wolfgang Sandner
Max-Born-Institut für Nichtlineare Optik und Kurzzeitspektroskopie, Max-Born-Straße 2 A, 12489 Berlin, Germany
(Received 23 November 2011; published 20 March 2012)

We present results of real-time tracking of atomic two-electron dynamics in an autoionizing transient wave packet in krypton. A coherent superposition of two Fano resonances is excited with a femtosecond extreme-ultraviolet pulse. The evolution of the corresponding wave packet is subsequently probed with a delayed infrared pulse. In our specific case, we get access to the interference between one- and two-electron excitation channels in the launched wave packet, which is superimposed on its decay through autoionization. A simple model is able to account for the observed dynamical evolution of this wave packet.

DOI: 10.1103/PhysRevLett.108.123601 PACS numbers: 42.50.Md, 32.80.Fb, 32.80.Zb

Investigating electron dynamics in an atom in the time domain, specifically when more than one electron is involved, directly gives insight into the electron correlation in the system. Dynamics has to be initiated with the absorption of light or by particle impact. Observation necessitates a second pulsed excitation of the system. This is usually done by two laser pulses, which can be precisely timed and made short enough to resolve the dynamic evolution of the system. Investigating two-electron dynamics requires the excitation of two electrons from an atom's ground state. These excited states are usually embedded in the ionization continuum, and decay through electron-electron correlation, e.g., into a ground-state ion and a free electron. Such a decay has been followed in real time for the first time by observing Auger-electron sidebands in a pump-probe experiment [1]. This experiment triggered several theoretical investigations that concern Auger decay [2,3] and continuum-electron dynamics in energy ranges that contain Fano-resonance structures in the absorption spectrum [4–7]. Fano resonances are induced by the presence of two-electron excited states, single inner-valence-electron excited states, or inner-shell-electron excited states that are embedded in the ionization continuum [8]. The dynamics of an electron wave packet that is launched in such an energy range therefore usually involves two-electron dynamics.

In this Letter, we investigate the evolution of a wave packet that is launched in the ionization continuum of krypton by an ultrashort extreme-ultraviolet (xuv) laser pulse (cf. Fig. 1). Within the spectral bandwidth of the xuv pulse, two Fano window resonances are found. One is induced by the inner-valence-electron excited configuration $(4s)^{-1}(7p)$, the second one by a two-electron excited configuration $(4p)^{-2}(nl)(n'l')$ (n, n': principal quantum numbers of the one-electron orbitals; l, l': their angular momenta) [9–11]. Both these excited configurations are embedded in the $(4p)^{-1}(\epsilon s/d)$ continuum (ϵ the energy of the photoelectron). In [10,11], the $(4s)^{-1}(7p)$ and $(4p)^{-2}(nl)(n'l')$ resonances have been labeled (14) and (15), respectively. We use this labeling here, too. The quantum numbers n, n', l, and l' of the latter configuration have not yet been identified in the literature. The angular momenta (l, l') are most likely of the type (s, p) or (p, d) and the principal quantum numbers $(n, n') = (5, 5)$ or $(5, 6)$ [9,10,12]. The wave packet dynamics after excitation by the xuv pulse is probed by the absorption of a photon from a delayed ultrashort infrared (ir) laser pulse. It photoionizes the $(4s)^{-1}(7p)$ orbital, with $(4s)^{-1}(\epsilon s/d)$ being the final continuum reached (Fig. 1), where the corresponding photoelectron is detected [13,14]. With this pump-probe scheme, we are able to look into the dynamics of this wave packet in real time. Specifically, we can follow the autoionization of the $(4s)^{-1}(7p)$ and $(4p)^{-2}(nl)(n'l')$ states, as well as the coherent two-electron dynamics that is expected to give rise to an interference between one- and two-electron excitation in the wave packet. Our

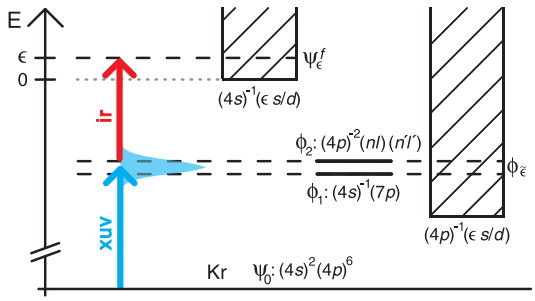

FIG. 1 (color online). The excitation scheme used for the real-time observation of two-electron dynamics. An xuv laser pulse launches a continuum wave packet in Kr with two Fano resonances participating. One is induced by an electron configuration with one inner-valence-electron excited, $(4s)^{-1}(7p)$, and the other one by a two-valence-electrons excited configuration $(4p)^{-2}(nl)(n'l')$. After a variable delay, the wave packet is probed by an ir laser pulse that induces a transition to the final $(4s)^{-1}(\epsilon s/d)$ continuum configuration.

investigation has an analogy in the decay of a core-excited Rydberg wave packet, which has been studied in [15].

The experimental setup has been described previously [16]. Briefly, Ti:sapphire (Ti:Sa) laser pulses [central wavelength: 787 nm (1.575 eV); bandwidth (full width at half maximum [FWHM]): 32 nm (64 meV); repetition rate: 1 kHz] with a pulse width of 40 ± 5 f sec were used to generate high-order harmonic pulses in Ar gas. Of the generated harmonics, only the 11th to the 21st ($H11$-$H21$) passed an aluminum-foil filter, and subsequently interacted with an effusive beam of Kr atoms within a magnetic-bottle photoelectron spectrometer. The wave packet of interest was started by the $H17$ harmonic content of the xuv beam [central wavelength: 46.3 nm (26.78 eV); bandwidth (FWHM, estimated from photoelectron kinetic-energy distributions): ≈ 0.5 nm (≈ 290 meV); pulse width: <30 f sec]. It covered the spectral range where the two window resonances, (14) and (15), are found in the photoionization continuum of Kr. They are located at 46.271 nm (26.795 eV) and 46.183 nm (26.846 eV), respectively. A small part of the Ti:Sa-beam was split off the main beam, and sent into a tunable delay line. These ir pulses served as probe pulses and ionized the launched electron wave packet. The magnetic-bottle spectrometer collected all photoelectrons that were generated in the focal spot, and directed them toward a microchannel plate detector. Their kinetic energy was calculated from the measured time of flight. At the laser beam focal spot, the ir pulses reached an intensity of $\approx 5 \times 10^{11}$ W/cm^2. The directions of polarization of the ir and the xuv beam were chosen to be parallel.

The ionization potential of the inner-valence $4s$ electron [$(4s)^{-1}(\epsilon s/d)$ ionization channel] is 27.511 eV [17]. Figure 2 shows the photoelectron kinetic-energy distribution in the energy range where we detect electrons in this channel after the absorption of one $H17$ and one ir photon. We show three spectra at different delay times δ. The negative delay in spectrum (a) refers to the ir arriving prior to the xuv pulse, while $\delta = 0$ in (b) represents the maximum temporal overlap. In spectrum (c), the ir probe pulse follows the xuv pulse.

In spectrum (a), we find only a delay-independent unresolved background of photoelectrons. This is caused by the harmonics $H19$ and $H21$, which travel with the xuv beam. Their photon energies exceed the photoionization threshold of a $4s$ electron, as well as the thresholds for the ionization of a $4p$ electron that leave Kr^+ in an excited electron configuration $(4p)^{-2}(nl)$ with $n > 4$ (see, e.g., [17]). These numerous high-lying ionic states give rise to a dense distribution of low kinetic-energy photoelectrons. The ir laser pulse is not involved in the generation of these photoelectrons.

With the laser pulses overlapping in time [Fig. 2, spectrum (b)], photoionization of the simultaneously excited wave packet by the ir laser pulse into the $(4s)^{-1}(\epsilon s/d)$ continuum sets in. Thus, an enhanced photoelectron yield in the energy range between ≈ 0.8 and ≈ 0.93 eV is detected. In the case of temporal overlap, there are two contributions to the electron yield in this spectral range. One, with a maximum at the low energy side of the spectrum at ≈ 0.83 eV, stems from photoionization of the wave packet. A second, spurious one, at the high energy side near 0.92 eV, is caused by sideband photoelectrons [18]. These have absorbed one photon from the $H11$ content of the xuv beam and emitted one ir photon, stimulated by the simultaneous presence of the ir laser pulse. They are ejected into the ionization channel that leaves the Kr^+ ion in the state $(4p)^{-1}\,{}^2P_{1/2}$. These two contributions cannot be separated while the laser pulses overlap in time.

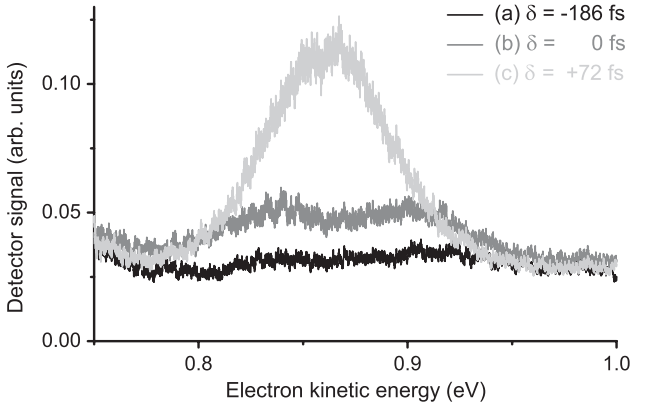

FIG. 2. Kinetic-energy distributions of photoelectrons in the $(4s)^{-1}(\epsilon s/d)$ ionization channel after absorption of one xuv and one ir photon. Spectra for three delay times δ are shown.

With the ir laser pulse following the xuv pump pulse [Fig. 2, spectrum (c)], the line that appears in the photoelectron kinetic-energy distribution originates solely from photoionization of the wave packet that has been launched by the $H17$ pulse. The broad spectral width of the ir pulse of 64 meV covered both window resonances, (14) and (15), which are separated by $\Delta E = 51$ meV [9]. Consequently, these are not resolved in the photoelectron kinetic-energy distribution. The significant photoelectron yield in the ionization channel $(4s)^{-1}(\epsilon s/d)$ for positive delays δ is caused by the finite time it takes an electron to leave the atom. This time is mainly determined by the lifetime of the bound configuration $(4s)^{-1}(7p)$ [11].

The dynamics of the launched wave packet is revealed when we take photoelectron kinetic-energy distributions in the ionization channel $(4s)^{-1}(\epsilon s/d)$ at a sequence of delay times δ. From the measured spectra we determined for each delay time the total photoelectron yield in the energy range depicted in Fig. 2. The resulting dependence of this photoelectron yield on δ is shown in Fig. 3(a). The delay $\delta = 0$, referring to maximum temporal pulse overlap, was determined by measuring the cross correlation of the xuv and ir laser pulses using a photoelectron sideband with contributions from the harmonics $H17$ and $H19$.

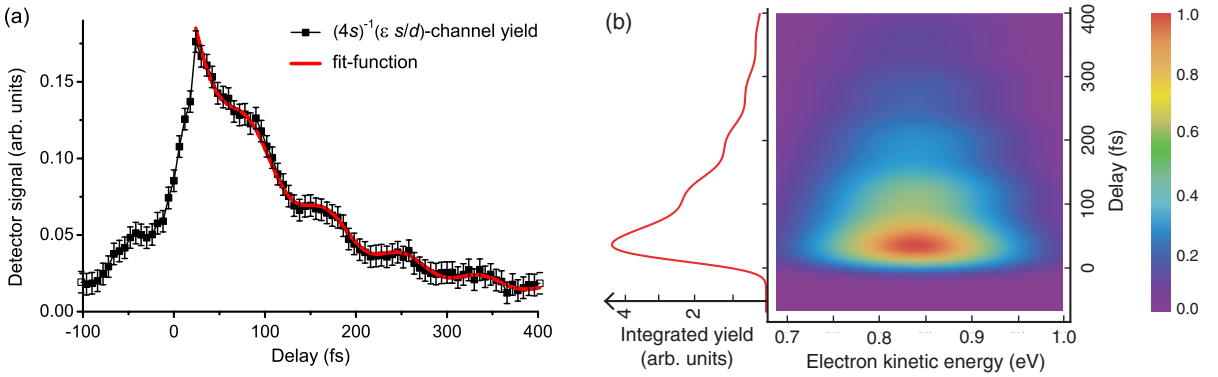

FIG. 3 (color online). (a) Dependence of the measured total photoelectron yield in the $(4s)^{-1}(\epsilon s/d)$ ionization channel on the xuv-ir delay δ (black squares). The added solid (red) line is a fit to the data using Eq. (1). (b) Two-dimensional density plot of the calculated photoelectron yield as a function of the photoelectron kinetic energy and of the pump-probe delay. On the left-hand side, the photoelectron yield is integrated over the energy range. The observed exponential decay, as well as the superimposed beating in (a) can be retrieved.

The excited wave packet is made up of a continuum configuration $(4p)^{-1}(\epsilon s/d)$ and contributions from the discrete configurations $(4s)^{-1}(7p)$ and $(4p)^{-2}(nl)(n'l')$. We expect these discrete state contributions to give rise to an oscillation imprinted on the photoelectron yield in the ionization channel $(4s)^{-1}(\epsilon s/d)$, when tuning the ir laser pulse delay. The period T of this oscillation is determined by the energy separation ΔE of the corresponding Fano resonances: $T = 2\pi\hbar/\Delta E \approx 81$ f sec [11]. The oscillation is expected to be superimposed on an exponential decay of the photoelectron yield, which is caused by the autoionization of the wave packet before it can be photoionized by the ir pulse. The decay is determined by the widths Γ_i of the two Fano resonances that contribute to the wave packet [$\Gamma_1 = 7.8$ meV for resonance (14); $\Gamma_2 = 3.5$ meV for resonance (15) [11]]. Precisely this behavior is found in Fig. 3(a). The quantum beats in the $(4s)^{-1}(\epsilon s/d)$ photoelectron yield clearly image the coherent two-electron dynamics in the wave packet. The wave packet's autoionization via the coupling of its discrete state admixtures to the Kr $(4p)^{-1}(\epsilon s/d)$ ionization continuum is reflected in the decay of the photoelectron yield with increasing delay δ.

A quantitative analysis of the delay dependence of the observed $(4s)^{-1}(\epsilon s/d)$ photoelectron yield can be based on a function $f(\delta)$ given by

$$f(\delta) = \exp(-\Gamma_1\delta/\hbar) + a\exp(-\Gamma_2\delta/\hbar) + b\exp\left(-\frac{\Gamma_1+\Gamma_2}{2\hbar}\delta\right)\cos(\Delta E\delta/\hbar + \phi). \quad (1)$$

The first two summands represent the autoionization decay of the two Fano resonances, while the third one describes the coherent oscillation between the two discrete electron configurations $(4s)^{-1}(7p)$ and $(4p)^{-2}(nl)(n'l')$. Its amplitude decays with the mean decay rate of the two resonances. Equation (1) was found to accurately fit the theoretical probe pulse delay dependence of the sideband photoelectron yield that was calculated for the photoionization of an atom by an xuv pulse in the presence of an intense long-wavelength pulse with two Fano resonances present in the energy range covered by the xuv light [6]. It is equally applicable to our experiment. The fit to our data is shown as a solid (red) line in Fig. 3(a). The parameters of the best fit are $\Delta E = 49 \pm 0.7$ meV, $\Gamma_1 = 5.6 \pm 0.15$ meV, $(\Gamma_1 + \Gamma_2)/2 = 3.2 \pm 0.8$ meV, $\phi = -0.15 \pm 0.15$, and $b = 0.067 \pm 0.01$. For the parameter a, the fit yielded a value close to zero with an error margin significantly larger than its value. This is expected from the already small b value, since a should be approximately equal to b^2. Because of this fact and the error margin of $(\Gamma_1 + \Gamma_2)/2$, it is not meaningful to determine Γ_2 from the fit. It is only possible to assert that Γ_2 is smaller than Γ_1. The extracted energy level difference of the discrete states ΔE agrees very well with the energy difference of the two Fano resonances (14) and (15) of 51 meV given in Ref. [11]. The width Γ_1, which we attribute to the $(4s)^{-1}(7p)$ resonance, however, shows a significant deviation from the value of 7.8 ± 0.8 meV, given in [11]. A similarly large deviation from these older results has recently also been reported in [13] for the width of the $(4s)^{-1}(6p)$ resonance in Kr.

A basic model is able to describe the observed electron dynamics. We assume a single final continuum, represented by states ψ^f_ϵ, with electron configuration $(4s)^{-1}(\epsilon s/d)$ (cf. Fig. 1). Also, the continuum wave packet that is launched by the xuv pulse is assumed to be composed of states $\psi_{\tilde{\epsilon}}$ of one single continuum. ψ^f_ϵ and $\psi_{\tilde{\epsilon}}$ are eigenstates of the full atomic Hamiltonian. The $\psi_{\tilde{\epsilon}}$ are assumed to be composed of two discrete states, ϕ_1 based on the electron configuration $(4s)^{-1}(7p)$, and ϕ_2 based on the configuration $(4p)^{-2}(nl)(n'l')$, and one continuum with states $\phi_{\tilde{\epsilon}}$ based on one of the configurations $(4p)^{-1}(\epsilon s/d)$. ϕ_1, ϕ_2, and $\phi_{\tilde{\epsilon}}$ diagonalize part of the atomic

Hamiltonian, with an interaction remaining between them. According to Fano, the $\psi_{\tilde{\epsilon}}$ can be expressed as linear superpositions of these states (see Ref. [8], Sec. 5),

$$\psi_{\tilde{\epsilon}} = a_1(\tilde{\epsilon})\phi_1 + a_2(\tilde{\epsilon})\phi_2 + \int d\epsilon' a(\tilde{\epsilon}, \epsilon')\phi_{\epsilon'}, \quad (2)$$

with the amplitudes a_i and $a(\tilde{\epsilon}, \epsilon')$ fixed by the remaining interactions among the ϕ_i and $\phi_{\tilde{\epsilon}}$. Deviating from Fano, we make a minor change in which we allow a direct interaction between the two discrete states ϕ_i $(i = 1, 2)$.

The transition matrix element $T_{f,i}$ from the atomic ground-state ψ_0 to the final ionization continuum ψ_ϵ^f is calculated by second-order time-dependent perturbation theory, which is sufficient for the ir light intensity in our experiment. It reads (assuming atomic units and neglecting an overall phase factor):

$$\begin{aligned} T_{f,i}(\delta, \epsilon) = \frac{1}{4} \int d\tilde{\epsilon} \langle \psi_\epsilon^f | D_2 | \psi_{\tilde{\epsilon}} \rangle \langle \psi_{\tilde{\epsilon}} | D_1 | \psi_0 \rangle \int_{-\infty}^{\infty} dt'' \\ \times \int_{-\infty}^{t''} dt' e^{i(\epsilon - \tilde{\epsilon} - \omega_I)t''} e^{i(\tilde{\epsilon} - \epsilon_0 - \omega_X)t'} \\ \times E_I(t'' - \delta) E_X(t'). \end{aligned} \quad (3)$$

Here, $E_I(t - \delta)$ and $E_X(t)$ are the amplitudes of the delayed ir probe and of the xuv pump pulse, respectively, and ω_I and ω_X are the corresponding carrier frequencies. Fano's theory allows us to give an explicit expression for the transition matrix elements appearing in $T_{f,i}(\delta, \epsilon)$ in terms of the parameters Γ and q of the involved resonances,

$$\begin{aligned} &\langle \psi_\epsilon^f | D_2 | \psi_{\tilde{\epsilon}} \rangle \langle \psi_{\tilde{\epsilon}} | D_1 | \psi_0 \rangle \\ &\quad = D \left(\sum_{i=1}^{2} \frac{p_i}{E_i} \right) \left(1 + \sum_{i=1}^{2} \frac{q_i}{E_i} \right) \Big/ \left[1 + \left(\sum_{i=1}^{2} \frac{1}{E_i} \right)^2 \right], \end{aligned} \quad (4)$$

with $E_i = (\tilde{\epsilon} - \epsilon_i)/(\Gamma_i/2)$, and q_i the Fano parameters describing the first step transition matrix element from the ground state to the continuum [based on Eq. (65) of [8]]. The ϵ_i are eigenvalues of the Hamiltonian 2×2 matrix that comprises the direct interaction of the discrete states ϕ_i $(i = 1, 2)$ and their second-order interaction via the continuum states $\phi_{\tilde{\epsilon}}$ [8]. Similar to the q_i parameters, the p_i characterize the ir-induced transition from the discrete states ϕ_i $(i = 1, 2)$ to the final continuum. In Eq. (4), the matrix elements coupling the $\phi_{\tilde{\epsilon}}$ continuum states to the final states ψ_ϵ^f are assumed to be zero. This is a reasonable assumption in our case. D can, for our purposes, be viewed as a proportionality constant. Equation (4) takes this simple form only, provided that all dipole matrix elements and all off-diagonal matrix elements in the above mentioned interaction matrix can be chosen to be real numbers.

Assuming the Fano parameters entering Eq. (4) are not energy dependent in the energy range covered by the bandwidths of the laser pulses, we calculated the transition probability $|T_{f,i}(\delta, \epsilon)|^2$ to the final continuum states ψ_ϵ^f as a function of the photoelectron kinetic energy ϵ, and of the delay δ. We used the Fano parameters ($q_1 = 0.11$, $q_2 = -0.38$) and Γ_2 (3.5 meV) from [11] and adopted Γ_1 (5.6 meV) from our measurement. The result of this calculation is shown in a two-dimensional density plot in Fig. 3. On the side, the kinetic-energy integrated delay dependence of the total photoelectron yield in the final continuum is plotted, which, for the parameters chosen in the calculation, matches reasonably the experimental result [cf. Fig. 3(a)]. The two-dimensional plot indicates that the amplitude of the oscillation that is superimposed on the decaying electron yield is a function of the photoelectron kinetic energy. This is expected and known from conventional quantum beats (see, e.g., [16]). Only at those kinetic energies where the quantum paths from the initial Kr ground state via the two Fano resonances to the final state ψ_ϵ^f are indistinguishable, quantum beats are expected to occur. The calculation reveals that the small oscillation amplitude of the photoelectron yield results from the fact that the transition amplitude from one of the Fano resonances to the final continuum is small compared to the other one. The transition amplitude ratio that results in the closest agreement of the calculated data with the measured ones in Fig. 3(a) is $p_2 = -0.05 p_1$. From the experiment, we expect the $(4p)^{-2}(nl)(n'l')$ resonance to be the weakly contributing one, since the transition to the $(4s)^{-1}(\epsilon s/d)$ continuum necessitates a two-electron transition.

In summary, we have presented the first experimental evidence of interference between one- and two-electron excitation channels in an atom in the time-domain. We employed a pump-probe scheme, where at least one of the discrete components of the intermediate continuum wave packet can be photoionized individually. The interference between the bound state components in the continuum wave packet causes quantum beats that appear along with the exponential decay of the autoionizing wave packet. In our specific case, this beating represents the energy exchange between two electrons in the Kr atom. Our technique complements the tracking of photoelectron sidebands, as it has been proposed in recent theoretical work [4–7]. It is of special value in the case of Fano window resonances contributing to the wave packet, where the sideband technique is difficult to apply. The technique can be used as a universal tool to get close insight into atomic two-electron dynamics.

We gratefully acknowledge funding from LASERLAB-EUROPE, Grant Agreement No. 228334, EC's Seventh Framework Program.

[1] M. Drescher, M. Hentschel, R. Kienberger, M. Uiberacker, V. Yakovlev, A. Scrinzi, T. Westerwalbesloh, U. Kleineberg, U. Heinzmann, and F. Krausz, Nature (London) **419**, 803 (2002).

[2] O. Smirnova, V. S. Yakovlev, and A. Scrinzi, Phys. Rev. Lett. **91**, 253001 (2003).
[3] C. Buth and K. J. Schafer, Phys. Rev. A **80**, 033410 (2009).
[4] M. Wickenhauser, J. Burgdörfer, F. Krausz, and M. Drescher, Phys. Rev. Lett. **94**, 023002 (2005).
[5] M. Wickenhauser, J. Burgdörfer, F. Krausz, and M. Drescher, J. Mod. Opt. **53**, 247 (2006).
[6] Z. X. Zhao and C. D. Lin, Phys. Rev. A **71**, 060702 (2005).
[7] W.-C. Chu and C. D. Lin, Phys. Rev. A **82**, 053415 (2010).
[8] U. Fano, Phys. Rev. **124**, 1866 (1961).
[9] K. Codling and R. P. Madden, Phys. Rev. A **4**, 2261 (1971).
[10] K. Codling and R. P. Madden, J. Res. Natl. Bur. Stand. Sect. A **76**, 1 (1972).
[11] D. L. Ederer, Phys. Rev. A **4**, 2263 (1971); **14**, 1936 (1976).
[12] H. Schmoranzer, A. Ehresmann, F. Vollweiler, V. L. Sukhorukov, B. M. Lagutin, I. D. Petrov, K. H. Schartner, and B. Möbius, J. Phys. B **26**, 2795 (1993).
[13] B. Doughty, L. H. Haber, C. Hackett, and S. R. Leone, J. Chem. Phys. **134**, 094307 (2011).
[14] B. Doughty, L. H. Haber, and S. R. Leone, Phys. Rev. A **84**, 043433 (2011).
[15] J. E. Thoma and R. R. Jones, Phys. Rev. Lett. **83**, 516 (1999).
[16] H. Geiseler, H. Rottke, G. Steinmeyer, and W. Sandner, Phys. Rev. A **84**, 033424 (2011).
[17] R. I. Hall, L. Avaldi, G. Dawber, M. Zubek, and G. C. King, J. Phys. B **23**, 4469 (1990).
[18] P. M. Paul, E. S. Toma, P. Breger, G. Mullot, F. Augé, P. Balcou, H. G. Muller, and P. Agostini, Science **292**, 1689 (2001).